Evaluation of the growth kinetics of θ' and θ-Al_2Cu precipitates in a binary Al-3.5wt%Cu alloy

Pierre Heugue[a], Daniel Larouche[a,*], Francis Breton[b], Rémi Martinez[c], X. Grant Chen[d]

[a]Laval University, Department of Mining, Metallurgy and Materials Engineering, Aluminum Research Center – REGAL, 1065, ave de la Médecine, Québec, Canada, G1V 0A6

[b]Rio Tinto, 1955, Mellon Blvd, Saguenay, Québec, Canada, G7S 4K8,

[c]Linamar Montupet Light Metal Casting, 32233 West Eight Mile Road, Livonia, MI, USA, 48152

[d]Université du Québec à Chicoutimi, Department of Applied Sciences, 555, boul. de l'Université, Saguenay, Québec, Canada, G7H 2B1

Corresponding author / E-mail address: Daniel.Larouche@gmn.ulaval.ca

Tel.:1-418-656-2153; Fax: 1-418-656-5343

Abstract

Heat treatment for precipitation hardening is known to have a large effect on the nano/micro-structure of cast aluminum alloys, and hence its properties. In the present work, precipitation kinetics after solutionizing and water quenching has been characterized by differential scanning calorimetry, transmission electron microscopy observations (TEM) and microhardness evaluations at different aging conditions. The Kissinger methodology was applied with the Lee-Kim-Starink-Zahra (LKSZ) kinetic equation in order to extract the kinetic parameters from DSC runs at constant heating rates, assuming that the precipitates have an ellipsoidal shape. TEM results showed evidence of semi-coherent θ' precipitation in accordance with the microhardness evolution during isothermal aging at 190°C and kinetic analysis from DSC data. The size and number density of precipitates were measured and counted on bright field TEM images taken on specimens aged at two different times. Activation energies for the precipitation kinetics of θ and θ' were found to be equal to 330 kJ/mol and 114 kJ/mol respectively. Finally, values for the interfacial mobility have been determined from the kinetic parameters derived from the DSC results and the TEM observations.

Keywords: Interfacial mobility; Differential Scanning Calorimetry (DSC); Precipitation Kinetics; Al-Cu Alloys

1. Introduction

The modeling of precipitation in metallic alloys has been the subject of many contributions in the past using diverse numerical approaches to predict the evolution of the size of the precipitates. The common ground of the vast majority of these models is to assume that the growth is controlled by diffusion (see [1, 2]). This mode of growth assumes that local equilibrium prevails at the interface and that the driving force is the concentration gradients in front of the precipitate. Considering that a mixed-mode control can provide a better ground to describe the growth of precipitates, Sietsma and van der Zwaag [3] concluded that the initial stage of each phase transformation is interface-controlled in all cases. This implies that the solute concentration in the matrix at the nucleus-matrix interface remains equal to the nominal concentration during the nucleation stage because of the large surface/volume ratio of the nucleus. Larouche [4] reaffirmed this concept by solving analytically the mixed mode growth of an ellipsoidal precipitate under the quasi stationary regime. Using as an example the case of an Al_2Cu-θ' precipitate growing in an aluminium matrix, the author showed that the calculated velocities in the early stage of growth can differ by a large factor from the values estimated by a diffusion control model. The difference can be particularly significant at low temperatures since the incubation regime may prevail during many hours. Moreover, the exact solution showed that at the start of the mixed mode regime, the interfacial concentration was equal to the nominal concentration, which means that the growth regime prior the mixed mode regime is interface controlled.

One of the challenges in modelling isothermal precipitation is getting a realistic value of the interfacial velocity at the start of the growth regime. If the calculated value overestimates the real one by a large factor, the end of the incubation regime will be poorly predicted since the error is impacting precisely the rate of fraction transformed. So, considering that the growth rate is interface controlled at the start of the growth regime, a large error can be made if one tries to estimate the interfacial velocity without consideration to the interfacial mobility, the latter depending on the activation energy for the migration of atoms across the interface. From this, we conclude that an accurate prediction of the isothermal evolution of the microstructure cannot be achieved if the interfacial mobility is unknown. Actually, the interfacial mobilities are unknown for age hardenable alloys.

In this paper, we will present a theory and an experimental procedure allowing a realistic evaluation of the interfacial mobility and its temperature dependency. This procedure will be applied to the θ' and θ phases growing in an Al-3.5wt%Cu alloy. Precipitation kinetics will be studied by the evaluation of the kinetic parameters obtained from the analysis of Differential Scanning Calorimetry (DSC) runs. The

interfacial mobilities will finally be estimated using the resulting kinetic parameters and the number density of precipitates determined from TEM observations.

2. Kinetic Model

i.Determination of kinetic parameters in solid phase transformation

A generic kinetic equation will be used to model the nucleation and growth of precipitates in a supersaturated matrix by associating the rate of the heat absorbed or released to the rate of phase transformed. The most versatile kinetic equation was proposed by Lee and Kim [5] and Starink and Zahra [6] (LKSZ). According to this equation, the time evolution of the fraction transformed α is given by:

$$\alpha = 1 - \left(1 + c \cdot (k \cdot t)^n\right)^{-\frac{1}{c}} \quad (1)$$

where t is the time and c, k and n are 3 independent kinetic parameters. For the precipitation of a phase θ in a supersaturated matrix, the fraction transformed is given by:

$$\alpha = \frac{g_\theta}{g_\theta^{eq}} \quad (2)$$

where g_θ and g_θ^{eq} are respectively the volume fraction and the equilibrium volume fraction of phase θ at a given temperature. The LKSZ equation encompasses the well-known equation proposed by Johnson–Mehl–Avrami–Kolmogorov (JMAK), the latter assuming that the interfacial velocity is constant. In order to associate the interfacial mobility with the kinetic parameters of the LKSZ equation, we have first to re-establish the LKSZ equation from the basic theory. The volume of an ellipsoidal precipitate θ growing with an interfacial velocity υ is given by:

$$V_{\theta(\tau)} = A_1 \cdot \left[\upsilon \cdot (t - \tau)\right]^3 \quad (3)$$

Where t is the time, τ is the incubation time and A_1 is related to the shape of the precipitate. In our development, we will assume that the ellipsoidal precipitate grows with constant eccentricities. This assumption maybe does not reflect perfectly the development of the plate shaped precipitates growing during the early stage of growth, but the error made is small considering that the volume fraction transformed is very small at this stage. Later, the precipitates generate ledges on every facets allowing growth in all directions. This makes the aspect ratio to stabilize somewhat as the precipitates evolve and

adopt the equilibrium shape. If a_1, a_2 and a_3 are the semi-principal axes of the ellipsoidal precipitate with $a_1 \geq a_2 \geq a_3$, then we have:

$$A_1 = \frac{4\pi}{3}\sqrt{1-e_{12}^2}\sqrt{1-e_{31}^2} \tag{4}$$

The eccentricities are related to the semi-principal axes by these equations:

$$e_{12} = \sqrt{1-\left(a_2/a_1\right)^2} \tag{5}$$

$$e_{31} = \sqrt{1-\left(a_3/a_1\right)^2} \tag{6}$$

Consequently, υ is equal to da_1/dt. Generic models are constructed by assuming that the volume is progressively filled by cells, each one containing one precipitate in equilibrium with the matrix included in the cell. The cell and its precipitate grow keeping their proportion so that the volume fraction *precipitate/cell* remains constant in each cell (under isothermal condition). The volume between the cells is the supersaturated matrix where nucleation of new cells is possible. Cells do not exchange atoms and Ostwald ripening is neglected. This assumption is justified in the context of a DSC analysis because it is expected that Ostwald ripening have a negligible effect on the heat released by the sample and will not change drastically the number density of particles during the growing stage of precipitation. The difference in chemical potentials between the supersaturated matrix and the cells drives the growth of the latest and their precipitates. At a given time t, we have:

$$\frac{dg_\theta}{d\tau} = I_V \cdot V_{\theta(\tau)} \tag{7}$$

where I_V is the rate of nucleation per unit volume. Now, we will develop a particular version of the LKSZ equation giving the possibility to associate experimental values to the kinetic parameters. Following the scenario explained by Larouche [7], we will assume that nucleation is a two-step process where, in the first step, the atoms quickly agglomerate on lattice defects and form a population of metastable embryos and, in the second step, the subcritical embryos experience ripening during which the losers are dissolving while the winners are growing steadily. The second step is called subcritical growth regime. In that stage, the winners are those growing at maximum speed, otherwise there are getting smaller than the winners, which eventually will impair their growth and promote their dissolution. Figure 1 depicts that situation, where one can easily acknowledge the concept of maximum growth velocity. It is worth to recall that in the classical nucleation theory (CNT), the growth rate is directly related to the frequency factor, the latter being not affected by the free surface energy.

Accordingly, one can expect that embryos emerging successfully from the nucleation stage are growing under the influence of the maximum driving force available. The capillarity forces may not have an impact on the growth rate of the winners, but will certainly affect the proportion of embryos having the critical size and the proportion of losers via the Zeldovich factor.

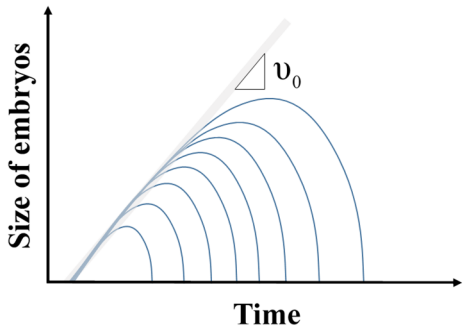

Figure 1: Schematic size evolution of a population of embryos during the subcritical growth regime

The number density of embryos reaching the critical size will be called N_0 and the time elapsed to reach this population will be neglected on the basis that the fraction transformed is still very small at this stage. Therefore, we will assume that time zero corresponds to the time where the precipitates nucleate spontaneously on N_0 heterogeneous sites, which is equivalent to say that nucleation sites are saturated at $\tau = 0$. Consequently, one can use the following relationship:

$$I_V = N_0 \cdot \delta(\tau) \tag{8}$$

where $\delta(\tau)$ is the Dirac delta function. The gradient of the chemical potential gradually decreases during the growth of precipitates; so one can assume that the velocity of the interface υ will decrease accordingly. Introducing the growth impingement exponent c, one can assume that the velocity can be estimated by the following equation:

$$\upsilon = \upsilon_0 \cdot \left(1 - \frac{g_\theta}{g_\theta^{eq}}\right)^{\frac{c+1}{3}} \tag{9}$$

where υ_0 is the interface velocity at the start of the transformation. This parameter is the interface migration velocity of the embryos emerging successfully from the nucleation process as schematized in Figure 1. It is expected according to Eq. (9), that the growth velocity $\rightarrow 0$ as the volume fraction g_θ is approaching the equilibrium volume fraction g_θ^{eq}. Inserting Eqs (2), (3), (8) and (9) into Eq. (7) and integrating from time 0 to t, one obtains:

$$\int_0^{\alpha} \frac{d\alpha}{(1-\alpha)^{c+1}} = \int_0^{t} \frac{N_0 \cdot A_1 \cdot \upsilon_0^3}{g_\theta^{eq}} \cdot \delta(\tau) \cdot (t-\tau)^3 \cdot d\tau \tag{10}$$

Since the Dirac delta function is by definition the time derivative of the unitary step function, it has the following property:

$$\int_{-\infty}^{+\infty} f(\tau) \cdot \delta(\tau) d\tau = f(0) \tag{11}$$

Therefore, one can show that the kinetic equation obtained from Eqs (10) and (11) is:

$$\alpha = 1 - \left(1 + c \cdot (k \cdot t)^3\right)^{-\frac{1}{c}} \tag{12}$$

Where:

$$k^3 = \frac{N_0 \cdot A_1 \cdot \upsilon_0^3}{g_\theta^{eq}} \tag{13}$$

Comparing Eqs (1) and (12), we see that the latter is a LKSZ kinetic equation, except that $n = 3$ and k is directly connected to the geometry of the precipitates, their number density, their initial growth velocity and the equilibrium volume fraction. From the kinetic equation, one can find the rate equation:

$$\frac{d\alpha}{dt} = 3k \left[\frac{(1-\alpha)^{-c} - 1}{c} \right]^{\frac{2}{3}} (1-\alpha)^{1+c} \tag{14}$$

The latter can be written as:

$$\frac{d\alpha}{f(\alpha)} = k(T) \cdot dt \tag{15}$$

where α, T and t are the independent variables from which the state of the system can be determined. Considering that the nucleation stage is completed at time zero and that the growth of a precipitate is a thermally activated process, the rest of the transformation can be modelled as a single stage reaction process for which k will have an Arrhenius type dependency with temperature:

$$k = k_0 \exp\left(-\frac{E}{RT}\right) \tag{16}$$

Kinetic equations describe isothermal transformation; but isochronal calorimetric analysis (constant heating rate) can be used to determine k_0 and E for a given $f(\alpha)$ with the variable state concept defined as [8]:

$$\omega = \int_0^{\alpha(t)} \frac{d\alpha}{f(\alpha)} = \int_0^t k_0 \exp\left(-\frac{E}{RT}\right) dt = \int_0^t k dt \tag{17}$$

Mittemeijer [9] was the first to use the so-called Kissinger methodology to extract the activation energy from DSC runs at different constant heating rates $\dot{T}$. For a fixed state of transformation ω_f, one can assign a temperature T_f so that:

$$\omega_f = \int_0^{\alpha_f} \frac{d\alpha}{f(\alpha)} \cong k_0 \frac{RT_f^2}{E\dot{T}} \exp\left(-\frac{E}{RT_f}\right) \tag{18}$$

By taking the natural logarithm on both sides of Eq. (18), one obtains:

$$R \cdot \ln\left[\frac{T_f^2}{\dot{T}}\right] = \frac{E}{T_f} - R \cdot \ln\left(\frac{R}{E}\frac{k_0}{\omega_f}\right) \tag{19}$$

The temperature at the top of a DSC peak can therefore be considered as the maximum rate of conversion. It corresponds to $\omega_f = \omega_{peak} = 1$ at $T_f = T_{peak}$. Examination of Eq. (19) reveals that the activation energy E can easily be determined from the slope of the curve obtained by plotting $R \cdot \ln\left(T_{peak}^2 / \dot{T}\right)$ as a function of $1/T_{peak}$,. The pre-exponential factor k_0 is evaluated from the intercept value occurring between the previous curve and the y-axis. The value of k in the LKSZ equation at different temperatures can then be well evaluated by this method. The impingement factor (c) can be estimated by fitting the LKSZ equation on the experimental DSC curve $d\alpha/dt$, the latter being determined from [10]:

$$\frac{d\alpha}{dt} = \frac{1}{\Delta h}(q - q_B) \tag{20}$$

where q is the power measured by the DSC, q_B is the baseline and Δh is the total latent heat released during the reaction. Fitting can be optimized using non-linear method of minimization of least squares error.

ii. Determination of the interfacial mobility

The mixed-mode growth regime starts at the end of the incubation regime during which many embryos have dissolved. The number density of embryos logically stabilizes when each embryo generates concentration gradients, which has for effect to isolate them from their neighbors. At this stage, one can assume that the fraction transformed is very small, so one may consider this time as the time zero of the reaction, where a stabilized number density N_0 of nuclei exists and begins the mixed-mode growth process. According to the theory presented in [4], the velocity of the boundary at the start of the mixed-mode regime of growth is given by :

$$\upsilon_0 = \frac{MRT}{V_m} \sum_{i=1}^{I} c_\theta^i \cdot \ln\left(\frac{\overline{c}_i}{c_{i\,eq}^*} \right) \tag{21}$$

where c_θ^i is the concentration of element i in the precipitate θ, V_m is the molar volume of the precipitate, M is the mobility of the interface, $\overline{c}_i$ is the nominal concentration of element i in the matrix, $c_{i\,eq}^*$ is the molar fraction of element i in the matrix which is in equilibrium with the precipitate and I is the number of species in the precipitate. Inserting Eqs (16) and (21) into Eq. (13), one obtains:

$$k = k_0 \exp\left(-\frac{E}{RT} \right) = \left(\frac{N_0 \cdot A_1}{g_\theta^{eq}} \right)^{1/3} \cdot \frac{MRT}{V_m} \sum_{i=1}^{I} c_\theta^i \cdot \ln\left(\frac{\overline{c}_i}{c_{i\,eq}^*} \right) \tag{22}$$

The interfacial mobility can be expressed as [11]:

$$M = \frac{\Omega}{RT} \exp\left(-\frac{E}{RT} \right) \tag{23}$$

From Eqs (22) and (23), one can see that the activation energy measured by the Kissinger method is the activation energy of the interfacial mobility, while the pre-exponential factor Ω is given by:

$$\Omega = \frac{V_m \cdot k_0}{\left(\frac{N_0 \cdot A_1}{g_\theta^{eq}} \right)^{1/3} \sum_{i=1}^{I} c_\theta^i \cdot \ln\left(\frac{\overline{c}_i}{c_{i\,eq}^*} \right)} \tag{24}$$

In the last equations, one can easily find values for A_1, V_m and c_θ^i knowing the nature and the shape of the precipitate. The variables $c_{i\,eq}^*$ and g_θ^{eq} can be evaluated at the specific temperature and nominal composition from the phase diagram or a thermodynamic computational tool. Finally, N_0 has to

be estimated from microscopic observations while E and k_0, have to be determined by kinetic analysis. Then, one obtains a first order estimation of the interfacial mobility and its temperature dependency. Notice that the above analysis implies that the activation energy is essentially related to the interfacial mobility and not to the coefficient of diffusion of solutes in the matrix. The impact of the latter is assumed to be accounted for by the c parameter, which mainly influences the rate at which the calculated fraction transformed evolves toward the equilibrium value past the peak temperature. Consequently, the interfacial mobility is thought as the parameter determining the onset temperature of a DSC peak while the coefficient of diffusion will determine the width of the DSC peak. This conclusion stands on the premise that beyond the peak temperature, the growth becomes more and more controlled by the diffusion.

3. Experimental methods

3.1. Sample preparation

About 31g of pure aluminum was melted in a ceramic crucible using an electrical resistance furnace. A controlled amount of pure Cu was added to the melt at 735°C to reach the desired chemical composition. The melt was mechanically stirred after copper addition and the melt surface was skimmed to eliminate the oxide layer. Sampling from the melt was carried out with Pyrex tubes equipped with a propipette. Tubes with a 5 mm inside diameter and 2 mm wall thickness were used for this purpose. Specimens were used for chemical analysis, phase identification in as-cast and solution heat treated (SHT) conditions, micro-hardness measurements, calorimetric testing and TEM observations at different aged conditions. The chemical composition of the alloys which was analyzed by atomic emission spectrometry (MP-AES 4100 from Agilent Technologies) is presented in Table 1.

Table 1: Chemical composition of cast Al-Cu alloy from cast ingots

	Elements	Si	Cu	Mg	Fe
Cast alloy	% wt	0.0055	3.4220	0.0012	0.0086
	±	0.0001	0.4542	0.0001	0.0020

The solution heat treatment (SHT) was conducted in an electric resistance furnace on small cylinders (20mm length). The temperature of the solution heat treatment, after a slow heating (~ 1h15m) was 500°C; a second step of SHT was applied at 550°C. For this two-step SHT, the time period of the first step at 500°C was ~ 8 hours, which was followed by ~8 hours at 550°C after 40 min of ramping up. After the 18 hours SHT, the specimens were quenched into cold water to obtain the maximum solute saturation. Disk shaped samples of 4.5 mm diameter and having a thickness of ≈ 2 mm were prepared

for DSC analysis from the quenched cylinders. The specimens were held for few hours at room temperature before their heating in the DSC device in order to limit the effects of natural aging.

3.2. Characterization methods

i. Microstructure and microhardness

Samples for microstructural and microhardness examination were sectioned from the quenched cylinder, mounted, ground, and polished using standard procedure. The polished sections were then evaluated with an optical microscope. Isothermal runs on selected samples were interrupted at 190°C in order to subject them to Vickers microhardness tests at room temperature. Microhardness experiments were conducted on Clemex CMT using a load of 0.0098 N with a dwell time of 13 s. To ascertain reproducibility and statistical validity, 10-16 microhardness tests were performed at each condition. Only intradentritic measurements were performed. Vickers microhardness indentations showing difference in the lengths of the diagonals over 5% of the mean were discarded. The typical accuracy as calculated from the standard deviation in a set of hardness data according to the number of indentations was about ±3 HV.

ii. Power Compensation Differential Scanning Calorimetry

Samples have been thermodynamically characterized by isochronal DSC analysis with the PerkinElmer Diamond instrument. The latter was calibrated for one heating rate (12.5°C/min). Measurements were conducted with all samples and references prepared with the exact same mass (±0.01mg). The instrumental baselines were performed with pure aluminum in the sample and reference furnaces for each heating rates. Figure 2 explains the methodology of the baseline graphical modifications to correct the results according to:

$$Q = (q - q_0) - q_0' \tag{25}$$

where q is the measured DSC result, q_0 is the measured instrumental baseline and q_0' is the calculated baseline with a polynomial function in accordance with [12].

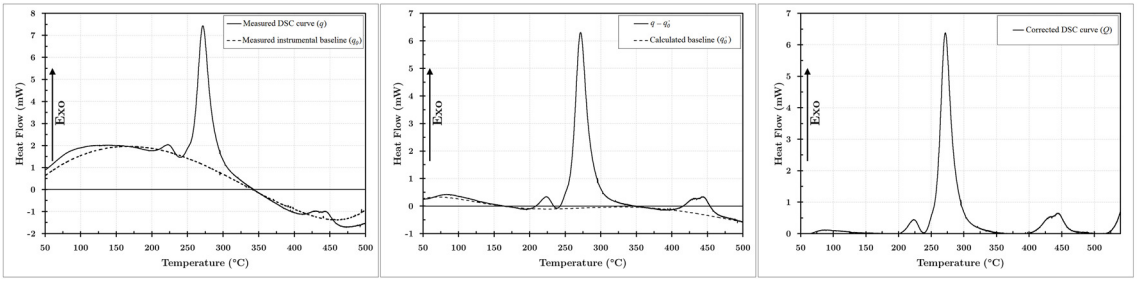

Figure 2: Baselines correction description for 80.55mg sample and reference with a 4K/min heating rate

Constant heating rates of 1, 2, 4, 5, 6, and 8 K/min were applied and two different samples were analyzed for each heating rate (except at 1 K/min) for reproducibility. Peaks identification has been done with literature comparison [13-20] for similar alloys and with temperature expectations from available metastable phase diagram.

iii. TEM preparation and observations

Two disks of ~ 1.2 mm thickness and ~ 4.5 mm diameter, with a weight equal to ~ 35 mg were cut from quenched cylinders and was heated at 150°C/min and aged at 190°C in the DSC furnace for optimized temperature control during 6h and 12h respectively. TEM samples have been prepared by electro-polishing from previous heat treated samples. Al_2Cu precipitates observations by transmission electron microscopy on Al matrix plans for the two different aging conditions have been done with a Jeol JEM-2100F TEM on 2F-1g or 2g matrix condition in g200 of aluminum near [001] axis and also in g200 near [011] axis.

4. Results

4.1. Microstructure observations and microhardness

As-cast microstructure (Figure 3-a) shows very low porosity but many stable θ-Al_2Cu intermetallic formed during solidification. After SHT (Figure 3-b), the microstructure becomes a homogeneous matrix with complete dissolution of θ-Al_2Cu intermetallics, which validates the SHT sequence for optimum aging. Line scan electron probe microanalysis revealed that the distribution of the elements was uniform in the dendrites after the SHT.

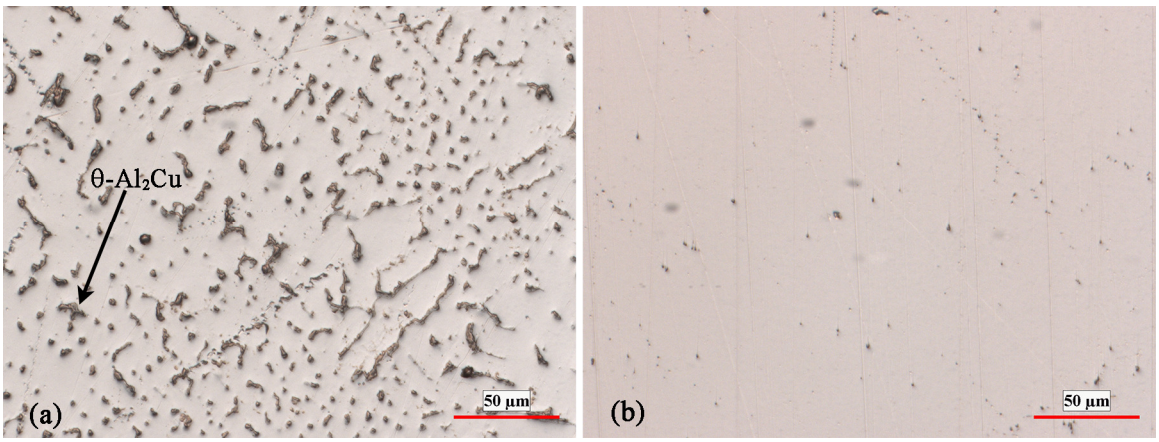

Figure 3: As-cast (a) and as-quenched (b) Al-3.5wt%Cu microstructure

Microhardness measurements on the alloy for different aging time at 190°C show changes in phase formation occurring between 6 and 10 hours due to a significant increase of the hardness (cf Figure 4).

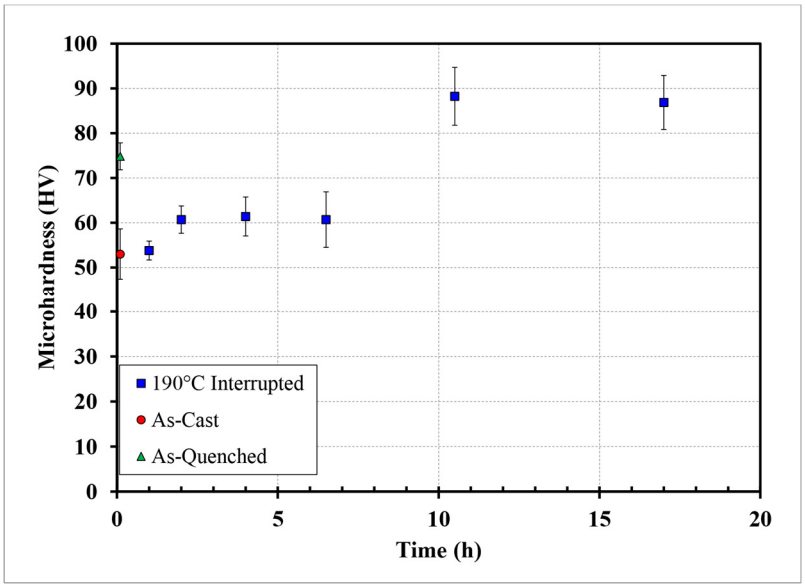

Figure 4: Microhardness evolution during aging at 190°C for the Al-3.5wt%Cu alloy

4.2. DSC runs for constant heating rate

The isochronal methodology developed in this study permits to obtain precipitation peaks for different constant heating as shown in Figure 5. The two graphs were obtained on different samples to check the reproducibility of the DSC results. The precipitation peaks have been identified according to literature and by comparison to the metastable phase diagram calculated by MatCalc v. 5.62 [21]. Three major peaks A, B, C have been studied corresponding to GP zones, θ' and θ formations respectively in the sequence of precipitation. The plots of the two graphs shown in Figure 5 differ only by the intensity of the peaks. The repeatability is very good regarding the onset and peak temperatures.

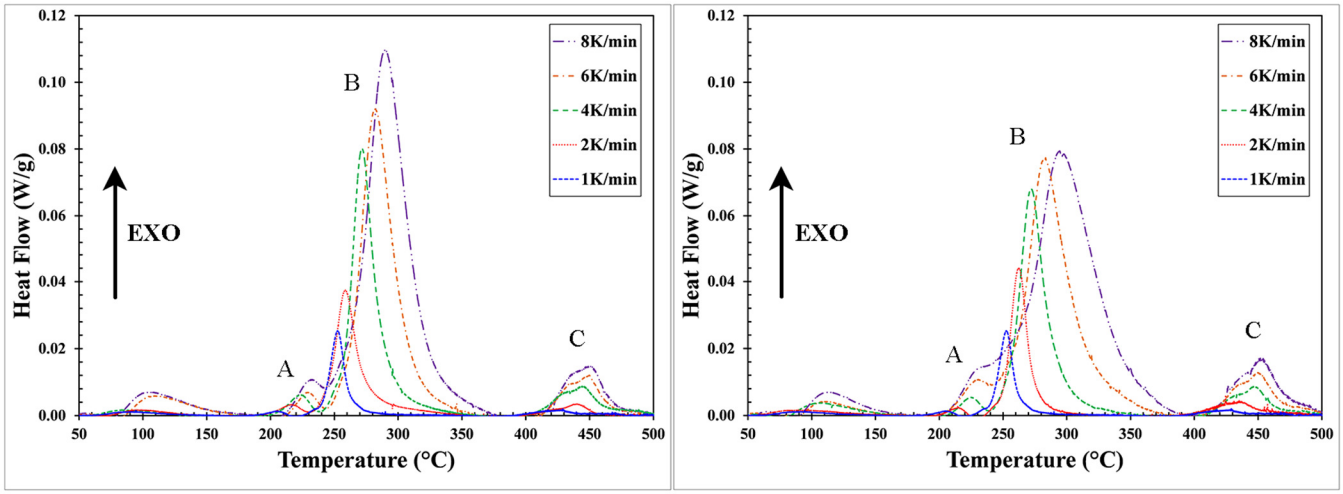

Figure 5: DSC runs for 1-2-4-6-8 K/min heating rates.

4.3. Determination of kinetic parameters by the Kissinger method

As described in the previous section, the Kissinger method was applied for precipitation kinetic analysis. Table 2 sums up the measured peak temperatures obtained with the different heating rates and Figure 5 presents the Kissinger diagrams for the three peaks.

Table 2: PC-DSC peak temperatures (°C) $T_f = T_{Peak}$ obtained at different heating rates on Al-3.5wt%Cu

Heating rate (K/min)	Peak A	Peak B	Peak C
1	205.6	252.5	414.1
2	214.5	262.4	423.2
	216.3	258.6	422.5
4	224.9	272.2	432.3
	223.2	271.7	430.7
5	228.4	286.0	433.7
	231.8	278.0	432.9
6	230.5	283.4	435.7
	229.2	282.2	435.2
8	239.8	294.5	439.3
	232.0	289.7	438.5

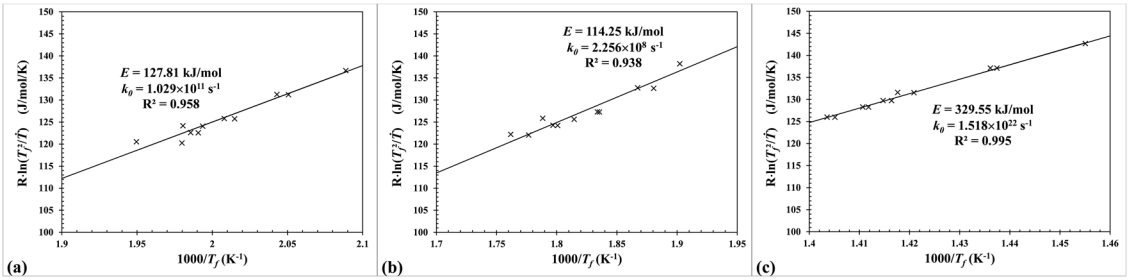

Figure 6: Kissinger diagrams for a) GP zones – peak A, b) θ'- peak B, c) θ – peak C

The values obtained for E and k_0 are presented in Table 3, which includes parameters c and Δh determined from the curve fittings made with different DSC curves.

Table 3: Parameters from the fitting procedure

Precipitate	E (kJ/mol)	k_0 (s^{-1})	n	c	Δh (J/g)
GP Zones	127.81	$1.029.10^{11}$	3	1	1.490
θ'	114.25	$2.255.10^{8}$	3	1.7	31.66 ±1.24
θ	329.55	$1.518.10^{22}$	3	4	3.476

The result of the curve fitting procedure is presented in Figure 7. Figure 8 displays the isothermal evolution of the fraction transformed at 190 and 350°C, as calculated with the LKSZ equation and the kinetic parameters given in Table 3.

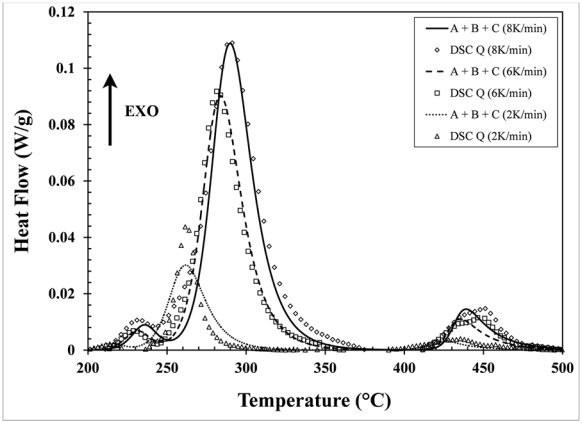

Figure 7: DSC runs and peaks adjusted to optimize the fit between experimental and sum of the heat produced by associated transformations

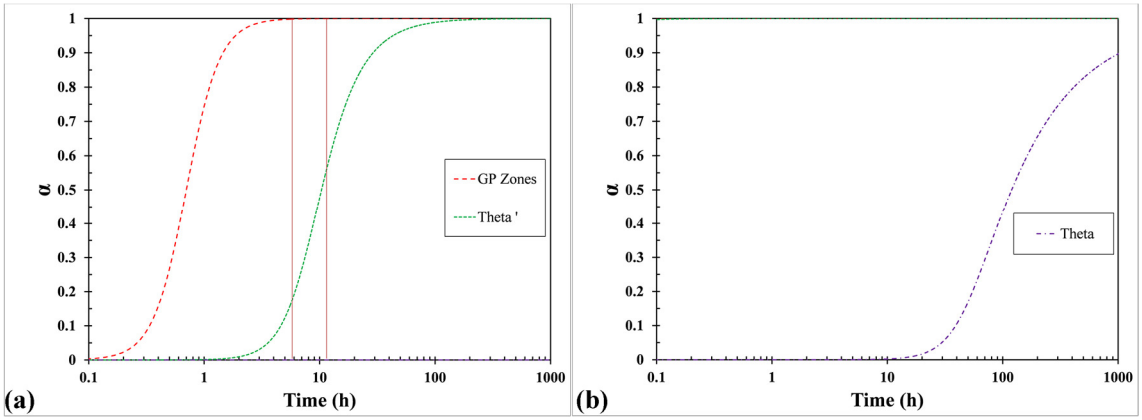

Figure 8: Isothermal evolution of the fraction transformed as calculated by the LKSZ kinetic model a) at 190°C and b) at 350°C

The calculated isothermal evolution of θ' at 190°C is in good agreement with the evolution of the heat flow measured in a differential Tian-Calvet isothermal calorimeter by Starink and Zahra [22] on an Al-4.4wt%Cu. According to their Figure 1, the heat flow starts to rise after 3 hours approximately and is close to completion after 100 hours. This precipitation time interval is close to the one shown in Figure 8. It is also interesting to notice that the rapid increase of the fraction transformed calculated between 6 and 12 hours (Figure 8) coincides with the rapid increase of microhardness (Figure 4).

4.4. TEM precipitate observations

Figure 9 and Figure 10 present the TEM bright field images recorded on the specimens aged at 190°C during respectively 6h and 12h. Notice that after 6h of aging at 190°C, the fraction transformed of θ' is only 17% according to the kinetic analysis (see Figure 8), so one can assume that the reaction is in its early stage of growth. The disk-shaped particles oriented perpendicularly one to each other are semi-coherent θ' metastable phase. The diffraction pattern visible in the white circles are typical of this

phase [23]. In some regions, some small incoherent stable precipitates (≤ 250nm in length) are present. These particles were identified as Al_2Cu-θ phase by Selected Area Electron Diffraction (SAED) analysis (Figure 11). The inter-reticular distances calculated from the diameters of the diffraction circle diameters give unit cell size dimensions of 0.407 nm and 0.601 nm, which are in agreement with those of the tetragonal crystal structure of this phase [24]. Length measurements of θ' precipitates were performed on 360 particles for each condition with the ImageJ software. Average lengths of 171.33nm ±68.91nm and 209.95nm ±80.48nm were obtained for aging time of 6h and 12h respectively.

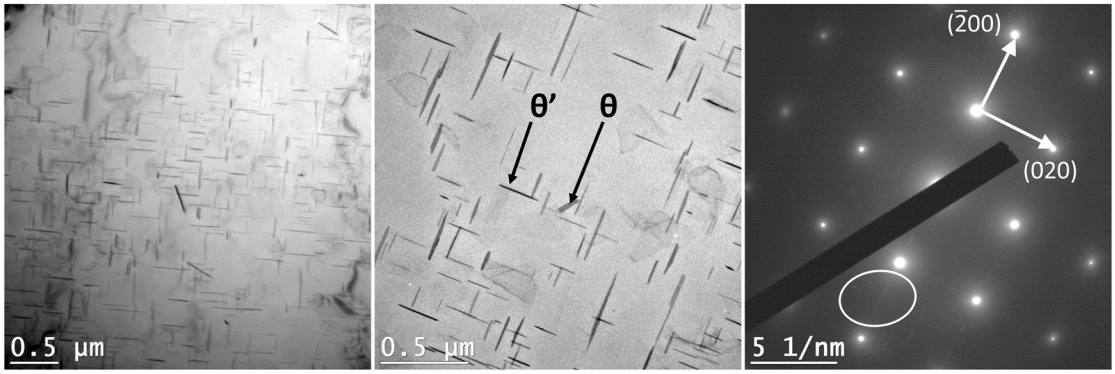

Figure 9: TEM observations along the <001> axis of a Al-3.5wt%Cu sample aged 6 hours at 190°C

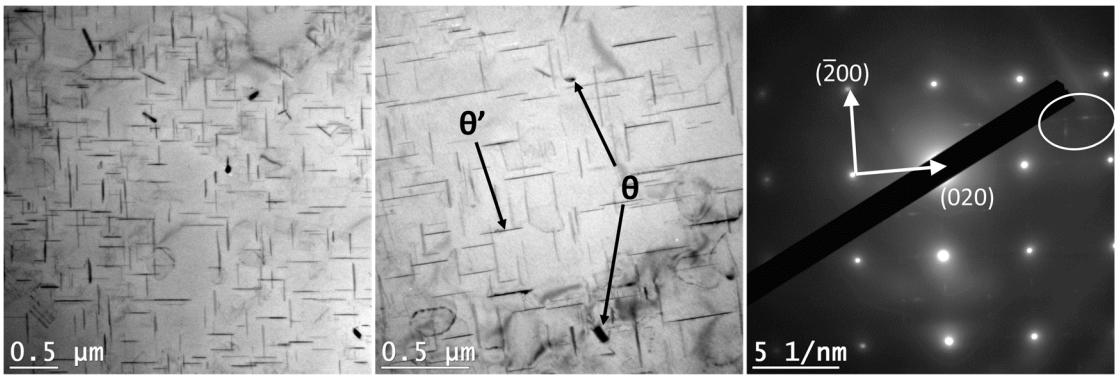

Figure 10: TEM observations along the <001> axis of a Al-3.5wt%Cu sample aged 12 hours at 190°C

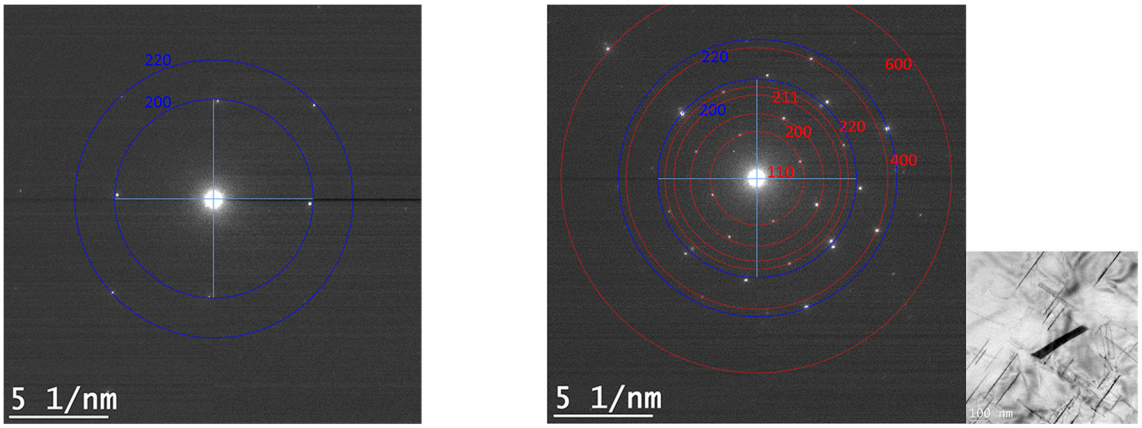

(a) **(b)**

Figure 11: SAED pattern on a) FCC Al matrix, b) θ-Al_2Cu tetragonal centered

In order to measure the precipitate number density in both conditions, the electron energy loss spectroscopy (EELS) Log-Ratio technique was performed in some areas to measure the local thickness of the TEM sample [25, 26]. The counting of θ' precipitates was realized in both perpendicular axis (*x*-axis, *y*-axis) on TEM pictures with the image analysis software. The average number of precipitates from both axes was multiplied by 3/2 in order to take into account θ' precipitates lying parallel to the plan of observation (*z*-axis). The number density was calculated by dividing the number of precipitates by the estimated volume and averaged over 8 different areas. Average number densities of 2.00×10^{20} particles/m^3 $\pm0.69\times10^{20}$ and 1.73×10^{20} $\pm0.46\times10^{20}$ were obtained respectively after 6 and 12h at 190°C. Because the number density of stable θ precipitates was much lower (an average number of 3 particles being seen per image), only one number density of this phase was made over the two aged conditions and the value obtained was 9 x 10^{18} particles/m^3. Notice that the value of Ω in Eq. (24) is inversely proportional to the cubic root of the number density, so a very accurate determination of the latter is not crucial for a first order estimation of the interfacial mobility.

4.5. Calculation of the interfacial mobility of θ and θ'

To calculate the interfacial mobility of θ and θ', one has to find the appropriate values for the parameters appearing in Eqs. (23) and (24). The parameter A_1, which is related to the shape of the particles, will be roughly estimated by assuming that the semi-coherent platelets of θ' and θ were growing as oblate spheroids having a typical aspect ratio of 20. The molar fractions $\overline{c}$ and $c^*_{i\,eq}$ and volume fractions ($g^{eq}_{\theta'}$ or g^{eq}_{θ}) were determined by assuming that the system was in equilibrium just before their respective onset temperatures. This condition was set on the basis that the optimum DSC scan must have a sufficiently high heating rate to get a clear peak when the phase transformation occurs and a sufficiently low heating rate in order that the phase transformation is 95% completed in a narrow temperature interval. Examination of the peaks obtained during the DSC runs reveals that the onset temperature was not strongly influenced by the heating rate. (See Figure 5). Moreover, as the heating rate is lower, the temperature interval of the peak is narrower, which is closer to the ideal condition where the transformation progresses in a quasi-isothermal mode. If low heating rates are best to characterize isothermal kinetic parameters, one may conclude that the samples were close to equilibrium just before the onset temperature. This condition is acceptable for almost all heating rates applied, even though some overlapping of the peaks occurred at the highest heating rate, considering that the onset temperatures obtained for a given peak are anyway close one to each other. The onset temperatures of the peaks associated to the θ' and θ phases were found to be respectively equal to 235 and 400°C. The

equilibrium values at these temperatures were calculated with MatCalc using the database assessed by Povoden-Karadeniz [27]. The results are given in Table 4**.** Notice that the Gibbs-Thomson effect was neglected, assuming that the particles size is in general sufficiently large at the end of the interface control growth regime to ignore the impact of the surface energy on the growth of the precipitate.

Table 4: Equilibrium values calculated with MatCalc for the alloy Al-3.5wt%Cu

T(°C)	Active Phases	$g_{\theta'}^{eq}$ or g_{θ}^{eq}	$c^{*}_{\mathrm{Cu}\ eq}$
235	FCC + θ'	0.0431	0.000843
400	FCC + θ	0.0295	0.00576

At 235°C, θ'' particles are dissolved under equilibrium condition according to MatCalc. The Cu molar fraction of the matrix at the onset temperature of θ' was then assumed to be equal to the nominal composition $\overline{c}$ = 1.517×10^{-2}. At 400°C, MatCalc predicts that θ' is not completely dissolved, and that the Cu molar fraction of the matrix is $\overline{c}$ = 7.788×10^{-3}. The molar fraction of Cu in the precipitates was c^{*}_{θ} = $c^{*}_{\theta'}$= 0.333 and the molar volume of precipitates was V_m = 1 x 10^{-5} m^3/mol. The site number density N_0 (number of sites per volume unit) was assumed to be equal to the number density of precipitates estimated from TEM observations made on samples aged at 190°C. These observations showed that the number density of the precipitates did not change significantly between 6 and 12 hours, which indicate that the reaction was under the growth regime during this period and that the effect of coarsening, due to overaging, was still not visible. The purpose of the Kissinger analysis is to provide the kinetic parameters giving the possibility to make comparisons between isothermal and isochronal aging. The sample produced after aging 6 hours at 190°C is theoretically in the same state as a sample having an equivalent fraction transformed after the onset of transformation occurring at 235°C during an isochronal treatment. This implies that the number densities measured at 190°C were certainly close to those obtained at the beginning of the peak occurring at 235°C during an isochronal heating. Notice that performing an isochronal aging until 235°C and then try to quench the specimen to obtain the TEM samples would have not been indicated because of the risks to get overaged specimens. Considering that the measurements of the number densities give a realistic but not a very accurate estimation of this parameter, the measured values were round off to one significant digit. So, N_0 values of 2 x 10^{20} sites/m^3 and 9 x 10^{18} sites/m^3 were used for θ' and θ respectively. Notice that the number densities of θ' measured after 6 and 12 h of aging do not differ when the values are reported with one significant digit. Finally, the appropriate kinetic parameter k_0 and E were taken from the results given in Table 3. Figure 12 presents the plots giving the relationship obtained between the interfacial mobility and the absolute temperature. The vertical bars represent the error margin introduced by a ±3°C uncertainty in the determination of peak temperature for the evaluation of E and k_0 according to the Kissinger analysis.

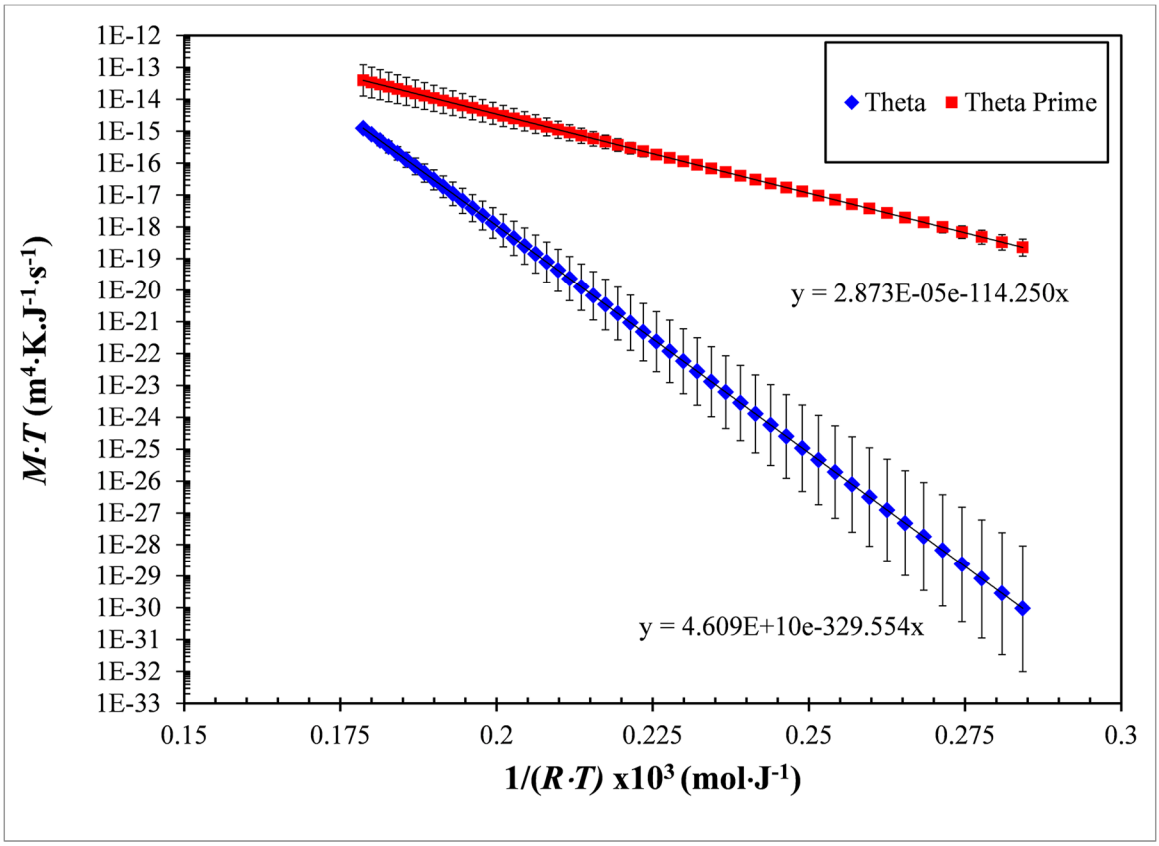

Figure 12: Diagram showing the temperature dependency of the interfacial mobility of phases θ and θ' in the Al-3.5wt%Cu alloy

5. Discussion

The results obtained with the DSC runs show a good reproducibility, though a slight difference in the peak amplitudes was observed (cf. Figure 5). This can be explained by a slight dissimilarity in quenching conditions between the two samples. Indeed, a slower quenching rate produces a lower amplitude of the exothermic peaks associated to the precipitation of secondary phases, as this was observed by Elgallad *et al.* [19]. Different values were reported in the literature for the activation energies associated to the precipitation kinetics of θ and θ' phases. The activation energies found in the present study are in agreement with these values, as this can be seen in Table 5.

Table 5: Activation energies for the formation of θ and θ' in different Al-Cu alloys from literature

Phase	Activation energy(kJ/mol)	Work	Alloy
θ'	*114*	This study	Al-3.5%Cu
	63-75	Fatmi *et al.* [17]	Al-3.7%Cu
	66-77	Elgallad *et al.* [19]	AA2219
	90±11	Mohammadian *et al.* [28]	Al-4.3%Cu
	98-108	Hayoune and Hamana [16]	Al-4.5%Cu

	100	Khamel *et al.* [29]	Al-3% Cu
	102-120	Fatmi *et al.* [30]	Al-2.4%Cu
	106	Starink and Van Mourik [14]	Al-4%Cu
	106-115	Wu *et al.* [31]	2519A
	109-117	Chen *et al.* [32]	Al-Cu-Mn
	119.5±8.3	Ovono et al. [20]	A319
	68 (DTA)	Wierszyłowski *et al.* [33]	Al-4.7%Cu
	101(dilatometry)	Wierszyłowski *et al.* [33]	Al-4.7%Cu
	330	This study	Al-3.5%Cu
θ	*200-360*	Elgallad *et al.* [19]	AA2219
	304	Wierszyłowski *et al.* [33]	Al-4.7%Cu

The activation energy associated to the precipitation kinetics of θ is approximately 3 times the value obtained for θ'. This large difference can hardly be explained by diffusion controlled mechanisms, considering that both phases have the same composition and have comparable surface energies according to Kozeschnik [1]. In a binary Al-3.5Cu, it is a fact that the onset temperature of the DSC peak associated to the θ' phase is well below the onset temperature of the DSC peak associated to the stable phase θ. The two phases have the same composition and the same atoms diffuse in the same matrix, so one cannot explain the large difference between the onset temperatures using arguments based on the diffusion of atoms in the matrix. The only possible explanation stands on the atomic attachment rate across the interface, which is exclusively related to the interfacial mobility. The two phases (θ and θ') differ by their crystallographic structure, their molar volume, their elastic properties and the nature of the interface (semi- coherent versus non-coherent). The interfacial mobility is ruled by the generation of new ledges and their migration rate. It seems obvious that the energy barrier to create a new ledge is much higher on the surface of a stable incoherent precipitates than it is for the metastable precursors, since the former have a crystal structure and molar volume differing much more from the matrix than the latter. The energy barrier for the migration of the ledge is probably higher also for the stable incoherent precipitate, though it is probably not the most important limiting barrier. The same reasoning can be made for all stable incoherent precipitates, which have a DSC peak occurring at higher temperature than their metastable semi-coherent precursors. One thing is sure. The wide difference between the activation energies cannot be explained by a diffusion controlled mechanism in the matrix, since the activation energies for the migration of one atom do not differ so much. The difference has to be accounted for by the energy of the system when it transits between a "flat" interface to one with a new ledge. Since this energy barrier is directly linked to the interfacial mobility, the activation energy measured by the Kissinger analysis is likely associated to the nucleation and migration kinetics of atomic ledges. This is why the activation energy of θ is 3 times higher than for θ'. The activation energy for the diffusion of Cu in Al, Q_{Cu}, is around 131 - 134 kJ/mol [34], which is a bit higher than the

activation energy of the interfacial mobilities for GP zones and θ'. This suggests that the migration of Cu atoms seems easier toward the metastable precipitates than toward the matrix, the common lattice structures helping the transfer up to a certain point. But Q_{Cu} is largely inferior to the activation energy of the interfacial mobility of the stable phase, which is 330 kJ/mole. The discontinuity of the lattices structures at the interface is making the transfer much more difficult.

The interfacial mobilities at the onset temperatures of θ' (235°C) and θ (400°C) are estimated by the proposed methodology to be respectively equal to 1×10^{-19} $m^4J^{-1}s^{-1}$ and 1.8×10^{-18} $m^4J^{-1}s^{-1}$. The corresponding radius growth velocities calculated with Eq. (21) are consequently equal to 4.1×10^{-11} m/s (148 nm/h) for θ' and 1.0×10^{-10} m/s (360 nm/h) for θ. Considering that the method gives a first order estimation of the interfacial mobility, one can say that interfacial velocities in the range 10^{-11} to 10^{-10} m/s correspond to a temperature above which the reaction rate increases exponentially and can be recorded as a peak by a power-compensated DSC. The evaluation of the interfacial mobility presented in this paper has some sources of uncertainties. Those associated with the number of sites (N_0) and the shape of the precipitates (A_1) have only a moderate impact on the interfacial mobility since the latter is inversely proportional to the cubic root of $N_0 \cdot A_1$. So, overestimating the value of $N_0 \cdot A_1$ by 100% produces an underestimation error of only 21% on the interfacial mobility. The most important uncertainty comes from the determination of the peak temperature. Depending on the data acquisition rate chosen in the DSC procedure, the noise or the time interval between the points is making some uncertainty on the exact position of the peak. The asymmetry of the peak, which may result from simultaneous dissolution-precipitation sequences, is also a source of error, especially when higher heating rates are applied. Fortunately, the endothermic peak amplitude of dissolving precipitates is much lower than the peak amplitude of growing precipitates since 1- the dissolution starts under quasi equilibrium conditions when the temperature is rising since the solubility of the matrix increases slowly with temperature as the latter is approaching the solvus and 2- the dissolution proceeds out of equilibrium once the solvus is crossed but with a very low driving force. The driving force acting on growing precipitates is much larger since the onset temperature is generally well below the solvus, the precipitation kinetic being activated when the thermal fluctuations are sufficiently high to propel the reaction. The endothermic reaction has however a clear effect on the shape of the DSC peak associated to the formation of θ and certainly on the true temperature where the precipitation kinetics reaches its highest conversion rate. A more sophisticated model, including the kinetics of all phases occurring simultaneously, would certainly give a more accurate determination of the parameters E and k_0.

6. Conclusion

The aim of this work was the development of a reliable method to characterize precipitation kinetics in Aluminium alloys in order to predict the incubation time and growth rate during isothermal aging. This was achieved by assuming that the early stage of growth is interface controlled, which implies that the kinetics of precipitation is governed by the interfacial mobility. This concept was proposed on the basis that the mixed mode growth (diffusion + interface control) is a more realistic approach than the diffusion controlled mode to estimate the evolution of a precipitate, since the interfacial mobility is not infinite, particularly at low temperatures.

The precipitation sequence in an Al-3.5wt%Cu has been investigated by DSC analysis and TEM observations. The results may be summarized as follows:

- DSC curves show up three major exothermic events, which were respectively identified to the formation of GP zones, θ' and θ.
- The activation energies associated to the precipitation of θ' and θ were found to be 114 and 330 kJ per mol respectively. These values are in agreement with previous evaluations made by other authors.
- The kinetic parameters estimated using the Kissinger methodology were associated to the interfacial mobility.
- TEM examinations showed a high number density of θ' precipitates and the presence of some isolated θ precipitates after 6h of isothermal aging at 190°C. The number density of θ particles was roughly 20 times lower than the number density of θ'.
- Finally, the interfacial mobility of θ' and θ precipitates has been evaluated with respect of temperature.

Acknowledgements

The authors would like to thank the Natural Sciences and Engineering Research Council of Canada (NSERC), Rio Tinto and Montupet for their financial support (NSERC Grant RDCPJ 468550 – 14). The authors are also grateful to K. Turgeon from Laval University for MP-AES analysis, and J.-P. Masse from (CM)² for TEM characterization.

Conflicts of Interest

The authors declare no conflict of interest.

References

[1] E. Kozeschnik: *Modeling Solid-State Precipitation*: Momentum Press, New York, NY, 2013, 464p.

[2] H. I. Aaronson, M. Enomoto, and J. K. Lee: *Mechanisms of diffusional phase transformations in metals and alloys,* Taylor & Francis, Boca Raton, FL, 2010, 667p.
[3] J. Sietsma and S. van der Zwaag: *Acta Mater.,* 2004*,* vol. 52, pp. 4143-52.
[4] D. Larouche: *Acta Mater.,* 2017, vol. 123, pp. 188-96.
[5] E. S. Lee and Y. G. Kim: *Acta Metall. Mater.,* 1990, vol. 38, pp. 1669-76.
[6] M. J. Starink and A. M. Zahra: *Thermochim. Acta,* 1997, vol. 292, pp. 159-68.
[7] D. Larouche: Phil. Mag., 2018, vol. 98, pp. 2035-60.
[8] M. J. Starink: *Int. Mater. Rev.,* 2013, vol. 49, pp. 191-226.
[9] E. J. Mittemeijer: *J. Mater. Sci.,* 1992, vol. 27, pp. 3977-87.
[10] S. P. Chen, K. M. Mussert, and S. van der Zwaag: *J. Mater. Sci.,* 1998, vol. 33, pp. 4477-83.
[11] J. W. Christian: *The theory of transformations in metals and alloys; an advanced textbook in physical metallurgy*, Pergamon Press,Oxford, UK, 1965, 973p.
[12] W. F. Hemminger and S. M. Sarge: *J. Therm. Anal.,* 1991, vol. 37, pp. 1455-77.
[13] S. K. Son, M. Takeda, M. Mitome, Y. Bando, and T. Endo: *Mater. Lett.,* 2005, vol. 59, pp. 629-32.
[14] M. J. Starink and P. Van Mourik: *Mater. Sci. Eng., A,* 1992, vol. 156, pp. 183-94.
[15] S. W. Choi, H. S. Cho, and S. Kumai: *J. Alloys Compd.,* 2016, vol. 688, pp. 897-902.
[16] A. Hayoune and D. Hamana: *J. Alloys Compd.,* 2009, vol. 474, pp. 118-23.
[17] M. Fatmi, B. Ghebouli, M. A. Ghebouli, T. Chihi, E.-H. Ouakdi, and Z. A. Heiba: *Chin. J. Phys.,* 2013, vol. 51, pp. 1019-32.
[18] S. Fu, D.-q. Yi, H.-q. Liu, Y. Jiang, B. Wang, and Z. Hu: *Trans. Nonferrous Met. Soc. China,* 2014, vol. 24, pp. 2282-88.
[19] E. M. Elgallad, Z. Zhang, and X. G. Chen: *Phys. B,* 2017, vol. 514, pp. 70-77.
[20] D. Ovono Ovono, I. Guillot, and D. Massinon: *J. Alloys Compd.,* 2007, vol. 432, pp. 241-46.
[21] E. Kozeschnik, J. Svoboda, P. Fratzl, and F. D. Fischer: *Mater. Sci. Eng., A,* 2004, vol. 385, pp. 157-65.
[22] M. J. Starink and A.-M. Zahra: *J. Mater. Sci. Lett.,* 1997, vol. 16, pp. 1613-15.
[23] D. G. Eskin: *J. Mater. Sci.,* 2003, vol. 38, pp. 279-90.
[24] D. A. Porter, K. E. Easterling, and M. Y. Sherif: *Phase transformations in metals and alloys*, 3rd ed, CRC Press, Boca Raton, FL, 2009, p.293.
[25] T. Malis, S. C. Cheng, and R. F. Egerton: *J. Electron Microsc. Tech.,* 1988, vol. 8, pp. 193-200.
[26] Y. Y. Yang and R. F. Egerton: *Micron,* 1995, vol. 26, pp. 1-5.
[27] E. Povoden-Karadeniz, *Thermodynamic Data from MatCalc Database 'mc_al.tdb',version 2.030,* 2015.
[28] H. R. Mohammadian Semnani and H. P. Degischer: *Kovove Mater.,* 2011, vol. 49, pp. 369–74.
[29] B. Khamel, F. Sahnoune, M. Fatmi, and N. Brihi: *Acta Phys. Pol., A,* 2017, vol. 131, pp. 133-35.
[30] M. Fatmi, B. Ghebouli, M. A. Ghebouli, T. Chihi, and M. Abdul Hafiz: *Phys. B,* 2011, vol. 406, pp. 2277-80.
[31] Y.-p. Wu, L.-y. Ye, Y.-z. Jia, L. Liu, and X.-m. Zhang: *Trans. Nonferrous Met. Soc. China,* 2014, vol. 24, pp. 3076-83.
[32] Z.-w. Chen, M.-j. Tang, and K. Zhao: *Int. J. Miner., Metall. Mater.,* 2014, vol. 21, pp. 155-61.
[33] I. Wierszyłłowski, S. Wieczorek, A. Stankowiak, and J. Samolczyk:,*J. Phase Equilib. Diffus.,* 2005, vol. 26, pp. 555-60.
[34] D. Simonovic and M. H. F. Sluiter, Phys. Rev. B, 2009, vol. 79, p. 054304.

Figure Captions

Figure 1: Schematic size evolution of a population of embryos during the subcritical growth regime

Figure 2: Baselines correction description for 80.55mg sample and reference with a 4K/min heating rate

552 Figure 3: As-cast (a) and as-quenched (b) Al-3.5wt%Cu microstructure

553 Figure 4: Microhardness evolution during aging at 190°C for the Al-3.5wt%Cu alloy

554 Figure 5: DSC runs for 1-2-4-6-8 K/min heating rates.

555 Figure 6: Kissinger diagrams for a) GP zones – peak A, b) θ'- peak B, c) θ – peak C

556 Figure 7: DSC runs and peaks adjusted to optimize the fit between experimental and sum of the heat
557 produced by associated transformations

558 Figure 8: Isothermal evolution of the fraction transformed as calculated by the LKSZ kinetic model a)
559 at 190°C and b) at 350°C

560 Figure 9: TEM observations along the <001> axis of a Al-3.5wt%Cu sample aged 6 hours at 190°C

561 Figure 10: TEM observations along the <001> axis of a Al-3.5wt%Cu sample aged 12 hours at 190°C

562 Figure 11: SAED pattern on a) FCC Al matrix, b) θ-Al2Cu tetragonal centered

563 Figure 12: Diagram showing the temperature dependency of the interfacial mobility of phases θ and θ'
564 in the Al-3.5wt%Cu alloy

565

566 **Table Captions**

567 Table 1: Chemical composition of cast Al-Cu alloy from cast ingots

568 Table 2: PC-DSC peak temperatures (°C) $T_f = T_{Peak}$ obtained at different heating rates on Al-3.5wt%Cu

569 Table 3: Parameters from the fitting procedure

570 Table 4: Equilibrium values calculated with MatCalc for the alloy Al-3.5wt%Cu

571 Table 5: Activation energies for the formation of θ and θ' in different Al-Cu alloys from literature

572

573

574

575

576

577

578

579

580